PROCEEDINGS OF SCIENCE

Gamma-Ray Bursts as Sources of Ultra-High Energy Cosmic Rays across the Ankle

Daniel Biehl[*,a], **Denise Boncioli**[b,c], **Anatoli Fedynitch**[d], **Jonas Heinze**[a], **Annika Rudolph**[a] **and Walter Winter**[a]

[a] *Deutsches Elektronen-Synchrotron (DESY), Platanenallee 6, 15738 Zeuthen, Germany*
[b] *Gran Sasso Science Institute (GSSI), Viale Francesco Crispi 7, 67100 L'Aquila, Italy*
[c] *INFN, Laboratori Nazionali del Gran Sasso (LNGS), 67100 Assergi, L'Aquila, Italy*
[d] *Dept. of Physics, University of Alberta, Edmonton, Alberta, Canada T6G 2E1*
E-mail: daniel.biehl@desy.de

The origin of Ultra-High Energy Cosmic Rays (UHECRs) is still unknown. Gamma-Ray Bursts (GRBs) are considered as potential sources as they belong to the most energetic events observed to date. However, conventional GRB scenarios are strongly constrained by the non-observation of associated astrophysical neutrinos. On the other hand, hidden accelerators such as low-luminosity GRBs (LLGRBs) can ameliorate the constraints. We show that the population of LLGRBs is not only consistent with current constraints, but can even describe the UHECR spectrum and composition across the ankle as well as neutrino data simultaneously. We explicitly compute the nuclear cascade in the source and stress that the sub-ankle component is directly related to nucleon and neutrino production in the nuclear cascade. We deduce source properties such as the baryonic loading or the cosmological event rate. Further, we study the impact of multi-zone models compared to the one-zone approach and how different collision dynamics change the predictions of GRB models.

36th International Cosmic Ray Conference – ICRC2019 –
July 24th – August 1st, 2019
Madison, WI, U.S.A.

*Speaker.

PoS(ICRC2019)196

1. Introduction

The sources of ultra-high energy cosmic rays (UHECRs) are still unidentified. However, advances in multi-messenger astronomy put the solution within reach by using combined information of disparate messengers such as cosmic rays, neutrinos, gamma rays and gravitational waves, which may originate from the same source. Due to UHECRs being measured up to energies of a few 10^{20} eV [1], they are presumably of extragalactic origin, as their Larmor radius is too big to be contained inside our galaxy. They are potentially accelerated in astrophysical objects releasing a vast amount of energy, of which one of the prime candidates were Gamma-Ray Bursts (GRBs) [2].

GRBs are among the most energetic electromagnetic outbursts observed to date, lasting from fractions of a second to hundreds of seconds. Because of their high energy output of 10^{53} erg and more, they were believed to be suitable acceleration sites for UHECRs. If there were in fact baryons involved, i.e., the burst is not purely leptonic, neutrinos would be almost inevitably produced in hadronic interactions of cosmic rays with ambient particles. However, until now, no neutrino event was detected in coincidence with a GRB, which puts stringent constraints on this population [3]. Viable scenarios for conventional GRBs require very low radiation densities, such that the UHECRs can escape from the source unscathed without producing neutrinos.

Nevertheless, the parameter space of conventional GRBs is largely excluded by neutrino stacking limits [4]. Low-luminosity GRBs (LLGRBs) emerge as a natural possibility to circumvent these constraints, as they are dim, which limits the detection of resolved sources, and usually long, making the background suppression less efficient. Their intrinsically low luminosity, being less than 10^{49} erg s^{-1}, further facilitates the escape of intact nuclei as well as low neutrino production. If LLGRBs are interpret as a distinct population from their high luminosity counterparts, their properties make them interesting candidates for UHECR and neutrino sources [5].

In this work, we study LLGRBs as a possibility to address the GRB-UHECR paradigm in a combined source-propagation model in the internal shock scenario. We introduce the concept of the nuclear cascade based on our previous work [4] and show how it develops in LLGRBs, leading to suitable cosmic ray compositions and neutrino fluxes for appropriate injection composition. Further, we perform extensive parameter space scans in which we attempt to simultaneously describe UHECR and neutrino data over a large energy range covering the ankle, where the cosmic ray spectrum changes its slope at $\sim 10^{18.7}$ eV. We show explicitly how the nuclear cascades controls the sub-ankle component, which leads to a smooth transition to a lower energy component, with which UHECR data can be reproduced across the ankle [6]. Finally, we discuss the prospects of GRBs in the light of multi-zone models and alternative collision dynamics.

2. Nuclear cascades in the parameter space

We assume a power law $\propto E^{-2}\exp(E/E_{\rm max})$ injection spectrum of primary nuclei from diffusive shock acceleration in the jet, for which the maximum energy $E_{\rm max}$ is determined by balancing acceleration and interaction rates, including synchrotron losses, photo-hadronic interactions and adiabatic cooling. The acceleration rate $t'^{-1}_{\rm acc} = \eta c/R'_L$ is parameterized by the Larmor radius $R'_L = E'/ZeB'$ of a particle with charge number Z and energy E' (in the shock rest frame). Further we use efficient acceleration, i.e., $\eta = 1$ throughout this work and assume that the magnetic field B'

is in equipartition with the energy density in gamma rays. The injection composition is chosen to be 60% ^{16}O and 40% ^{28}Si, motivated by the composition given in [7] (*cf.* Si-R 1), which seems plausible for GRB progenitors such as Wolf-Rayet stars. Note that the acceleration efficiency and the composition (along with the energy scale uncertainties of Auger) are degenerate. For the prompt emission phase, the target photon field is modeled as a broken power law with spectral indices $\alpha = 1.0$ and $\beta = 2.0$ below and above the break energy of $\varepsilon'_{\gamma,\mathrm{br}} = 1$ keV. According to the internal shock model, accelerated nuclei interact with these photons at a distance $R \simeq 2\Gamma^2 ct_v$ from the central engine. In the following, we fix the Lorentz factor to $\Gamma \simeq 10$ and vary the radius between 10^8 km and 10^{12} km, with corresponding changes in the variability time t_v.

The nuclear interactions within LLGRB jets are calculated with *NeuCosmA* [4], which is based on CRPropa 2 ($A < 12$) [8] and TALYS ($A \geq 12$) [9] for photo-disintegration (photon energy in nucleus' rest frame $\varepsilon_\gamma \lesssim 150$ MeV) and on SOPHIA [10] for photo-meson production ($\varepsilon_\gamma \gtrsim 150$ MeV), where we apply a superposition model for nuclei, i.e., $\sigma_{A\gamma} \approx A\sigma_{p\gamma}$. Due to such photo-nuclear interactions, accelerated primary nuclei can break up and produce lighter secondary particles in what is called the nuclear cascade. The corresponding interaction rates are directly proportional to the radiation density

$$u'_\gamma = \int \varepsilon' N'_\gamma(\varepsilon') d\varepsilon' = \frac{L_\gamma}{4\pi c \Gamma^2 R^2} \quad , \tag{2.1}$$

such that the luminosity L_γ and the emission radius R are the main control parameters for the development of the nuclear cascade. In the left panel of Fig. 1, we performed a classification of the parameter space according to qualitatively different nuclear cascade regions. For low radiation densities, the nuclear cascade cannot fully develop in the source. This case is called "Empty Cascade", for which the source is optically thin to photo-hadronic interactions of all species. As a consequence, only a few secondary isotopes, nucleons and neutrinos are produced. Increasing the radiation density leads to the "Populated Cascade" region, where interactions become efficient for heavy masses. As a consequence, many different nuclear species are populated, including moderate production of nucleons and neutrinos. For even higher densities, the source becomes opaque even for nucleons, called "Optically Thick Case". In this case, the disintegration of nuclei is so efficient that most of the energy is dumped in nucleons, which comes with high neutrino production. We also show the maximum energy of the injected primary, indicated by the dashed gray contours, which is limited by adiabatic cooling in the Empty Cascade region and by photo-hadronic interactions in the region where the cascade develops (and hence the tilt). We show different bench marks depicted by point A, B and C in the parameter space in the following, whereas point Z refers to [7].

The ejected cosmic ray spectra are parameterized as $\propto \exp(-\ln^2(E/E_{\max}))$, meaning that cosmic rays escape from the source only at the highest energies [11]. This leads to hard spectra which is generally favorable for the fit to cosmic ray data. The output of our source model is then processed by the propagation model, for which we use *SimProp* [12] with the extragalactic background light from [13] and the TALYS photo-disintegration model [9]. The cosmological distribution of LLGRBs is given by $(1+z)^m \mathscr{H}_{\mathrm{SFR}}(z)$ relative to the star formation rate (SFR) [14], where we consider $m = 1$ in this work. In the last step, we perform a fit to the UHECR spectrum [1] and composition [15] by fitting the super-ankle component ($> 10^{19}$ eV) first, and then introducing an additional power law component at lower energies (sub-ankle) to describe the transition across

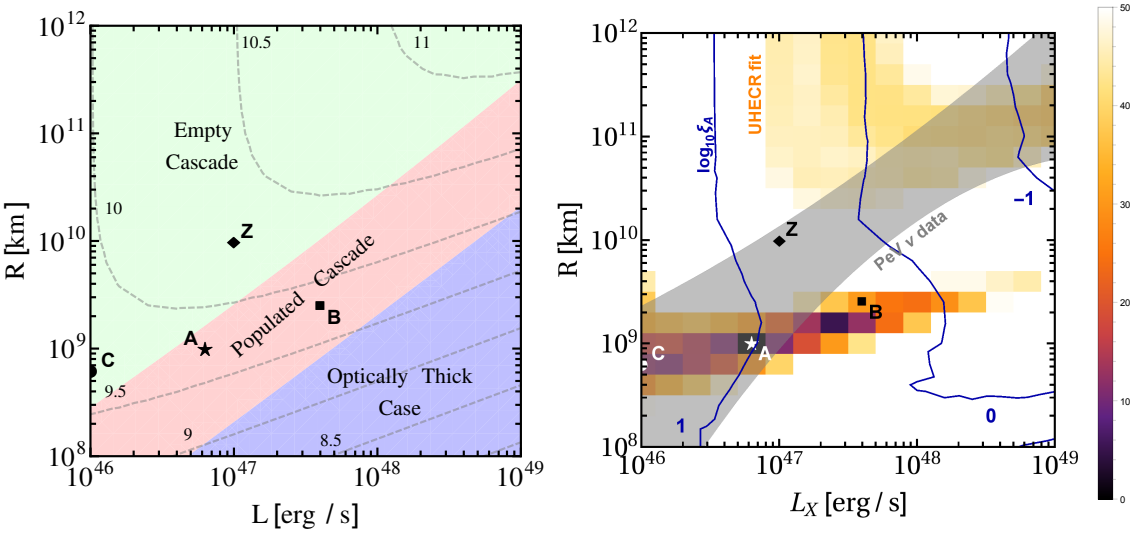

Figure 1: Parameter space study of the nuclear cascade (left panel) and the UHECR fit (right panel) as a function of luminosity and collision radius for pure ^{28}Si injection. The nuclear cascade regions correspond to the different cases described in the text and the superimposed contours represent the maximum energy for the injected isotope in the shock rest frame $\log_{10}(E_{\rm max}/{\rm GeV})$. The results of the fit to UHECR data are shown by the color scale displaying $(\chi^2 - \chi^2_{\rm min})$. The region suitable to describe neutrino PeV data within their 1σ uncertainties is depicted by the gray band. The blue curves indicate the baryonic loading $\log_{10}\xi_A$ obtained from the fit. In both panels, point A represents the best fit to data, points B and C are additional bench marks with similar maximum energy and point Z indicates the example shown in [7]. Taken from [6].

the ankle. The relative weights of both components are then re-fit in order to obtain a description covering the whole energy range above 10^{18} eV. The baryonic loading is then evaluated a posteriori from the normalization of the fit. Note that the baryonic loading is degenerate with the duration T_{90} and the local rate of LLGRBs. The results of this procedure are shown in the right panel of Fig. 1, where we show the quality of the fit to UHECR data as indicated by the color scale. The region for which the data is best reproduced follows the maximum energy along $E_{\rm max} \simeq 10^{9.7}$ GeV in the source. In addition, the superimposed dark region represents parameter combinations for which the resulting source neutrino flux is within the 1σ uncertainties of the IceCube PeV data [16]. This also shows that in order to account for IceCube PeV neutrino data, at least a moderate amount of interactions is required, as this region clearly falls in the Populated Cascade region. The best fit point is named A indicated by the star, wheres B and C serve for demonstration purposes in the following. The dark blue contours show the baryonic loading $\log_{10}\xi_A$ obtained from the fit, which interestingly agrees with typical values from the literature as $\xi_A \sim 10$ at the best fit. Note that the baryonic loading is degenerate with the local rate and duration of LLGRBs.

3. UHECR fit results across the ankle

The results for UHECR and neutrino observables obtained at the best fit point A are shown in Fig. 2, which illustrates that both, cosmic ray and neutrino data can be described simultaneously at the highest energies. For the cosmic ray observables, the solid orange curve represents the

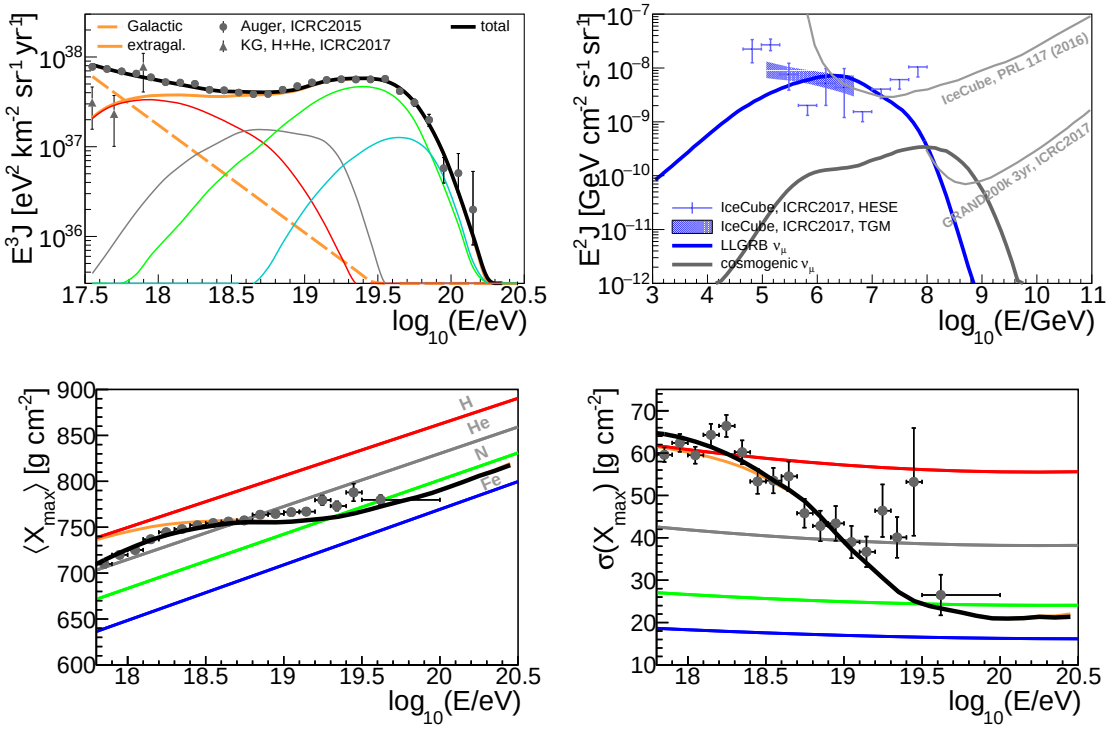

Figure 2: Cosmic ray spectrum (top left) and composition (bottom) and diffuse neutrino fluxes (top right) over energy for the best fit point A in Fig. 1. The energy spectrum of UHECRs, multiplied by E^3, shows the contribution to the total spectrum (black) by the extragalactic component (solid, orange) as well as a sub-ankle component (dashed, orange), which could be a residual galactic power law. For the extragalactic component, the contribution of different mass groups is illustrated too (thin, red $A = 1$, gray $2 \leq A \leq 4$, green $5 \leq A \leq 24$, cyan $25 \leq A \leq 28$). The data points represent the results from Auger [1] and KASCADE-Grande (for the light component, H and He) [17]. Similarly, the composition observables show the extragalactic contribution (solid, orange) and the total including a heavy sub-ankle component. For comparison, predictions of EPOS-LHC [18] are shown as well. The predicted muon neutrino spectrum (blue) is compared to IceCube data from High Energy Starting Events (HESE, blue data points) and Through Going Muons (TGM, blue band) [16]. The corresponding cosmogenic neutrino spectrum (gray) is compared to limits from IceCube [19] and GRAND [20]. Taken from [6].

contribution of the extragalactic component only (mass group splitting according to the caption), while the solid black also includes a residual power law at low energies (which may be of Galactic origin). Even though reproducing the spectra with a one-source population above EeV energies is possible [4], it is hard to describe the UHECR composition, as nucleons dominate below the ankle and thus the composition would be too light. Hence, the sub-ankle power law is assumed to be heavy, e.g., $A = 28$ in this example, with a spectral index of $\alpha = 4.2$ and a fraction of $\sim$ 78% of the corresponding flux at $E = 10^{17.5}$ eV obtained from the fit. These values also depend on the source evolution, as a higher value of m results in a larger nucleon flux at low energies due to interactions during the propagation and vice versa. Furthermore, cosmogenic neutrinos are expected to be detected from such a population of LLGRBs with next generation instruments. However, it decreases by a factor of ~ 2 if SFR is used ($m = 0$).

The nuclear cascade directly controls the extragalactic sub-ankle nucleon component and the source neutrino fluxes. The points A, B and C corresponding to the markers in Fig. 1 represent parameter combinations which lead to a similar cut-off energy in the cosmic ray spectrum. While point B has a larger radiation density compared to the best fit point A, the nucleon flux below the ankle is enhanced and the super-ankle component is accordingly depleted due to strong interactions. For the same reason, more source neutrinos are produced. In turn, point C shows a lower radiation density, leading to smaller nucleon and neutrino fluxes. As cosmogenic neutrinos are more sensitive to the maximum cosmic ray energy than to the radiation density in the source, the predicted flux is similar among these bench marks.

4. Multiple and ultra-efficient shocks

Instead of assuming a static burst with a number of identical collisions $N = T_{90}/t_v$ in the shock rest frame, we now allow for a dynamical evolution of the burst. This means that each of these collisions has different radiation parameters, i.e., luminosity, Lorentz factor and collision radius. At the end of the simulation, the output of all collisions will be summed up to obtain the total ejected spectrum of a GRB. As a consequence, there may be objects which are both, efficient neutrino producers and cosmic ray emitters at the same time, as collisions may occur at large and small radii, with correspondingly high and low radiation densities, to a similar extent. The impact of these model assumptions are important for the viability of conventional GRB scenarios, as it was believed that multi-zone models potentially yield lower neutrino fluxes [21]. However, this typically depends on the engine behaviour, which in a simple picture emits shells of material with different speeds, separation and thickness. These shells represent spatial fluctuations of the mass density ejected by the central emitter, which collide during the evolution of the GRB fireball due to non-vanishing relative Lorentz factors. If the engine is irregular or stochastic, collisions tend to be more optically thick to photo-hadronic interactions, as the relative Lorentz factors of two neighboring shells tend to be larger than in the case of disciplined engines.

Each collision can be categorized according to the nuclear cascade such that, in the end, the distribution among the different scenarios describes the expected output. From our simulations, we expect that even in the case of disciplined engines, the conventional GRB-UHECR paradigm can be constrained by neutrino data in the multi-zone model in the coming years [25]. However, collision dynamics could also have an impact on the results. The standard assumption is that shells collide inelastically, i.e., merge after they collide as their internal energy is radiated away [26]. An ultra-efficient shock scenario, in which a fraction of the energy is converted into kinetic energy such that the shells do not merge but separate after the collision [23], has been tested (among others) in [24]. This changes the collision distribution as a function of the dissipated energy and the collision radius for the GRB, as shown in Fig. 3. The left panel illustrates the standard scenario, for which the collisions are almost Gaussian distributed in dissipated energy and collision radius, with most collisions happen at intermediate radii. Such collisions are expected to be somewhat optically thick to photo-hadronic interactions, resembling the characteristics of the Populated Cascade.

On the other hand, the ultra-efficient shock case is depicted in the right panel, for which most collisions occur at large radii, but the dissipated energy for these collisions is very low. This is a consequence of more shells being available further outside of the fireball, leading to more

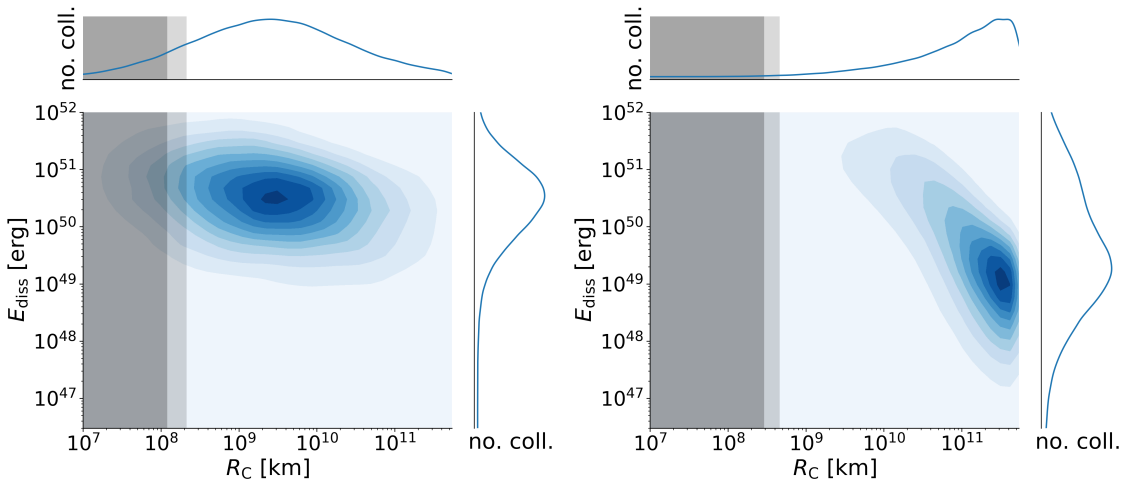

Figure 3: Number of collisions as a function of the dissipated energy and the collision radius for inelastic shell collisions (standard case, left panel, corresponding to GRB 1 in [22] with $E_{\gamma,\rm iso} = 5.2 \cdot 10^{52}$ erg and constant mass injection rate) and ultra-efficient shocks (right panel, corresponding to [23]). The contours illustrate the density of the number of collisions. Taken from [24].

collisions, however their relative Lorentz factors are small due to prior collisions, resulting in low interaction rates. The output is still dominated by the fewer collisions at intermediate radii, where shells collide for the first time with higher relative Lorentz factors, such that most of the energy is dissipated there. In total, the cosmic rays can reach slightly higher maximum energies, but the neutrino flux remains comparable. Moreover, hydrodynamical simulations with PLUTO [27] have shown that ultra-efficient shocks occur rarely ($\sim 10\%$ of all collisions), as it is only possible under very specific conditions. In conclusion, the standard scenario of inelastic collisions is a reliable assumption and collision dynamics do not have a large impact on the predictions. For a detailed review, see [24].

5. Conclusion

The conventional GRB-UHECR paradigm is under serious tension due to the non-observation of associated neutrinos. While the parameter space is largely excluded, recent studies point towards LLGRBs as a viable possibility to avoid these constraints. We studied this scenario in a combined source-propagation model including nuclear cascades within the source environment. The parameter space can be categorized by means of nuclear cascade development and we show that it is possible to describe UHECR spectrum and composition across the ankle as well as PeV neutrino data simultaneously with sources which are moderately intransparent to photo-hadronic interactions. As a consequence of the local rate and long duration of these objects, we find baryonic loadings of ~ 10 at the best fit.

Further, we investigate the impact of multi-zone models on the results and conclude that even in the dynamical fireball model, GRBs are under growing tension by neutrino data. The predictions depend mostly on the engine behaviour in that case, of which disciplined engines typically lead to lower neutrino fluxes due to their lower relative Lorentz factors. Different engine properties lead

to different shapes of the corresponding light curves, such that electromagnetic observations could be one possibility to characterize central emitter.

Alternative collision dynamics have a rather small impact on the predicted cosmic ray and neutrino fluxes. Ultra-efficient shocks were found to be rare and affect only the interior processes in the fireball. In general, inelastic shell collisions are a reliable assumption. Other model components, as e.g. the cosmic ray escape mechanism, may have a much larger influence on the results. For different escape assumptions, the spectral index of the ejected spectrum can vary greatly, making a fit to data much more challenging. Nevertheless, a multi-zone LLGRB model would be an interesting application to further study these objects.

Acknowledgements. This project has received funding from the European Research Council (ERC) under the European Union's Horizon 2020 research and innovation programme (Grant No.646623).

References

[1] I. Valiño for the Pierre Auger Collaboration. PoS(ICRC2015)271, 2015.
[2] T. Piran. *Rev. Mod. Phys.*, 76:1143–1210, 2004.
[3] R. Abbasi et al. *Nature*, 484:351–353, 2012.
[4] D. Biehl et al. *Astron. Astrophys.*, 611:A101, 2018.
[5] K. Murase et al. *Phys.Rev.*, D78:023005, 2008.
[6] D. Boncioli et al. *Astrophys. J.*, 872(1):110, 2019.
[7] B. T. Zhang et al. *Phys. Rev.*, D97(8):083010, 2018.
[8] K.-H. Kampert et al. *Astropart. Phys.*, 42:41–51, 2013.
[9] A. J. Koning et al. *EDP Sciences*. volume vol. 211, 2008.
[10] A. Mucke et al. *Comput. Phys. Commun.*, 124:290–314, 2000.
[11] Y. Ohira et al. *Astron. Astrophys.*, 513:A17, 2010.
[12] R. Aloisio et al. *JCAP*, 1210:007, 2012.
[13] R. C. Gilmore et al. *Mon. Not. Roy. Astron. Soc.*, 422:3189, 2012.
[14] A. M. Hopkins et al. *Astrophys. J.*, 651:142, 2006.
[15] A. Porcelli for the Pierre Auger Collaboration. PoS(ICRC2015)420, 2015.
[16] C. Kopper for the IceCube Collaboration. PoS(ICRC2017)981, 2017.
[17] D, Kang for the KASCADE-Grande Collaboration. *PoS*, ICRC2017:452, 2018.
[18] T. Pierog et al. *Phys. Rev.*, C92(3):034906, 2015.
[19] M. G. Aartsen et al. *Phys. Rev. Lett.*, 117(24):241101, 2016.
[20] K. Fang et al. *PoS*, ICRC2017:996, 2017.
[21] N. Globus et al. *Mon. Not. Roy. Astron. Soc.*, 451(1):751–790, 2015.
[22] M. Bustamante et al. *Astrophys. J.*, 837(1):33, 2017.
[23] S. Kobayashi et al. *Astrophys. J.*, 551(2):934–939, apr 2001.
[24] A. Rudolph et al. *in preparation*.
[25] J. Heinze et al. *in preparation*.
[26] S. Kobayashi et al. *Astrophys. J.*, 490:92–98, 1997.
[27] A. Mignone et al. *Astrophys. J. Suppl.*, 170(1):228–242, may 2007.